Remote Sounding of Cirrus Cloud Optical Depths and Ice Crystal Sizes from AVHRR Data: Verification Using FIRE II IFO Measurements

S. C. OU,* K. N. LIOU,* Y. TAKANO,* N. X. RAO,* Q. FU,* A. J. HEYMSFIELD,†
L. M. MILOSHEVICH,# B. BAUM,# AND S. A. KINNE@

*Department of Meteorology/CARSS, University of Utah, Salt Lake City, Utah.
†NCAR, Boulder, Colorado.
#Atmospheric Sciences Division, NASA/Langley Research Center, Hampton, Virginia.
@NASA/Ames Research Center, Moffett Field, California.

(Manuscript received 15 June 1994, in final form 2 September 1994)

ABSTRACT

Using the data obtained from the Advanced Very High Resolution Radiometer (AVHRR) 3.7-μm and 10.9-μm channels, a retrieval scheme has been developed to simultaneously infer cirrus cloud optical depth and mean effective ice crystal size based on the theory of radiative transfer and parameterizations. A numerical scheme is further developed to remove the solar component in the 3.7-μm radiance for applications to daytime satellite data. This scheme is based on the correlation between the 3.7-μm (solar) and 0.63-μm reflectances. Validation of the algorithm has been performed by using various datasets that were collected during the FIRE-II IFO (Nov–Dec 1991) at Coffeyville, Kansas. We have focused on the 26 November and 5 December cases. The retrieval analysis over a 0.5° × 1.0° area is performed around Coffeyville for each case based on AVHRR-HRPT data. For validation the authors analyze the photomicrograph data collected by the balloonborne replicator, determine the microphysical and optical properties of the sampled cirrus clouds, and derive their position at the satellite overpass based on sounding data. It is demonstrated that the retrieved cirrus cloud temperature, mean effective ice crystal size, and optical depth closely match the observed values. Further, the retrieved cirrus cloud properties are applied to the computation of surface radiative fluxes using a radiative transfer program that involves a consistent representation of cirrus cloud fields. The computed values are compared with the data measured from ground-based radiometers, and it is shown that the computed downward surface IR and solar fluxes are within 5 and 10 W m^{-2} of the measured values, respectively, near the time of satellite overpass.

1. Introduction

Cirrus clouds are globally distributed, primarily present in the upper troposphere and lower stratosphere, and are composed almost entirely of nonspherical ice crystals. Information on cirrus cloud microphysical and optical parameters is critically important to the development of cirrus forecast models, the upgrading of real-time global cloud analysis, the computation of the radiative energy budget of the earth–atmosphere system, and the investigation of cloud feedbacks in global climate change (Liou 1986).

In our recent paper (Ou et al. 1993), we developed a physical retrieval scheme using radiance data from AVHRR 3.7-μm and 10.9-μm channels to infer nighttime cirrus cloud parameters, including cloud temperature, optical depth, and mean effective ice crystal size, based on the theory of radiative transfer and parameterizations. This retrieval scheme has been applied to the nighttime AVHRR satellite data collected at 0930 UTC 28 October 1986 over Wisconsin during the First ISCCP Regional Experiment, Phase I, Cirrus Intensive Field Observation (FIRE-I IFO). Verifications have been carried out for the retrieved cloud temperature/height and mean effective ice crystal size over a 1° × 1° area west of Fort McCoy against lidar and in situ aircraft measurements. We show that the satellite-retrieved mean cloud heights differ from the lidar values by less than 0.5 km and that the retrieved mean effective ice crystal size is within 5 μm of the values derived from the in situ aircraft measurements.

For daytime retrievals a numerical scheme for removing the solar component in the 3.7-μm radiance has been developed (Rao et al. 1995). The resulting removal–retrieval program has also been applied to the AVHRR data collected at 2100 UTC, 28 October 1986, over Wisconsin during FIRE-I IFO. For verifications and comparisons of retrieval results, Table 1 lists the retrieved mean values of cloud temperature, cloud height, and optical depth over small areas near the three FIRE-I IFO stations: Madison (MAD), Fort McCoy (FMC), and Wausau (WAU). Also listed are the cloud temperature and midcloud height, both of which are

Corresponding author address: Dr. Szu-Cheng Ou, Dept. of Meteorology/CARSS, University of Utah, 809 William C. Browning Bldg., Salt Lake City, UT 84112.

© 1995 American Meteorological Society

TABLE 1. Cirrus cloud temperature, mean effective ice crystal size, cloud height, and optical depth determined from the present retrieval program.

Station	T_c (K)		D_e (μm)	z (km)		τ	
	Present	Lidar[a]	Present	Present	Lidar[a]	Present	GOES[a]
WAU	226.5	230.7	57.1	9.5	9.0	1.54	1.43
FMC	229.7	226.5	61.3	9.1	9.5	1.5	1.41
MAD	225.6	228.1	53.9	9.6	9.3	0.6	0.56

[a] After Minnis et al. (1990a).

derived from collocated and coincident lidar and sounding data. The lidar-derived parameters are based on the average data within ±15 min of 2100 UTC. The optical depth is retrieved from the GOES data obtained at the same time as the *NOAA-9* overpass (Minnis et al. 1990a,b). Retrieved cloud temperatures and cloud heights at all three stations agree reasonably well with those derived from lidar measurements. The differences may be caused by the effects of the vertical inhomogeneity within cirrus clouds. The retrieved optical depths differ from those derived from the GOES data by less than 0.15.

Validation of the satellite remote sensing technique for the retrieval of cirrus cloud parameters requires ground and air truth data that are available from a composite field experiment. In addition to our efforts cited above, Minnis et al. (1990a, 1993) have used ground-based lidar measurements collected during FIRE-I IFO to verify the retrieved cirrus cloud height. Baum et al. (1994) have also presented comparison results for the satellite-retrieved and lidar, radar, and aircraft-measured cloud heights, using data collected during FIRE-II IFO. However, attempts to validate the retrieved optical depths and ice crystal sizes using in situ data have not been made at this point. There are two primary requirements. To evaluate the cirrus cloud vertical optical depth, continuous microphysical measurements in the vertical must be available. Moreover, to minimize the effects of horizontal inhomogeneity, the cloudy region sampled by the in situ instruments must correspond to that viewed by the satellite.

In this paper we have carried out a more comprehensive validation for the retrieved cirrus cloud optical depths and mean effective ice crystal sizes, using the *NOAA-11* AVHRR data, the balloonborne replicator data, and the NCAR-CLASS (Cross-chain LORAN Atmospheric Sounding System) sounding measurements that were obtained during FIRE II IFO. The advantage of using the replicator data is that the replicator sondes will provide a continuous record of the cloud microphysical properties in the vertical. Thus, it is possible to determine the optical depth and vertically averaged mean effective ice crystal size. Furthermore, we have also used the retrieved cirrus cloud optical depths and mean effective ice crystal sizes in conjunction with a radiative transfer parameterization program to compute the surface radiative fluxes, which are subsequently compared with the ground-based radiometer measurements that were obtained during FIRE-II IFO. These comparisons will thus provide a consistent check on the retrieved cloud parameters, on the one hand, and the radiation parameterization program on the other.

This paper is organized as follows. In section 2 we describe the various datasets that are used in the validation program. The removal–retrieval scheme and the evaluation of the optical depth and mean effective ice crystal size from the replicator data are presented in section 3. Section 4 presents the retrieval analyses and verification results associated with the two cases selected. Finally, conclusions are given in section 5.

2. Data sources

The FIRE-II IFO was carried out near Coffeyville, Kansas, during November and December 1991. One of the objectives of this field experiment is to quantify the capabilities and limitations of methods for retrieving physical and optical cirrus cloud properties from satellite observations. During the latter part of November and the first part of December 1991, a total of 11 cirrus days were observed. For all these cases we have reviewed the available satellite data and lidar measurements as well as examined the temporal differences between the satellite overpass time and the sampling time of the sounding system. From lidar measurements for cirrus clouds it has been shown that the backscattering coefficients varied significantly in space as constructed from the time series of backscattering returns (J. Alvarez 1993, personal communication). We have found that around 2100 UTC on both 26 November and 5 December there were well-defined cirrus cloud layers over the Coffeyville area and that the temporal differences between the satellite overpasses and replicator measurements were less than 30 minutes. Thus, we have focused on these two dates for the retrieval analyses and verifications.

For the retrieval of cirrus cloud properties high-resolution AVHRR data from *NOAA-11* satellite are used. This satellite has nominal equator crossing times of 0140 and 1340 LST. The AVHRR is comprised of five channels: 0.63, 0.8, 3.7 (NIR), 10.9 (IR), and 12 μm. The NIR and IR radiances were calculated from the

raw counts provided in the *NOAA-1B* data stream using the nominal calibration (Kidwell 1991) and from the nonlinearity corrections described by Weinreb et al. (1990). The visible channel radiances were calculated using the instrument degradation correction function provided by Whitlock et al. (1990).

Balloonborne Formvar (Polyvinyl formal) ice crystal replicators were launched during FIRE-II IFO to measure the "vertical profiles" (in a Lagrangian sense) of cirrus microphysical properties, with emphasis on the detection of small ice particles. Schaefer (1941) first developed the Formvar replication technique to capture and preserve detailed features of snowflakes, using a solution of Formvar dissolved in ethylene dichloride. Particles falling onto a solution-coated slide or filmstrip are enveloped by fluid, forming a detailed replica of the particle when the solvent evaporates and the plastic hardens. The use of Formvar replication on a balloonborne instrument, that is, a "replicator sonde," was developed by Magono and Tazawa (1966) to study the vertical distribution of snow crystals up to the 500-mb level in a snow cloud. The fundamental design of the ice crystal replicator employed in FIRE-II IFO was based on the prototype developed by Magono and Tazawa, with modifications to improve the data quality and to allow the instrument to collect data in high and cold cirrus clouds.

Replicator launches were timed to coincide with satellite overpasses and during the time periods when ground-based remote sensors and aircraft were operating. The replicators were launched together with the NCAR CLASS and then tracked and retrieved by an automobile using the radio direction finding equipment. The balloon size and inflation were chosen to deliver an ascent rate of about 5 m s^{-1} and to burst at 11–13-km altitude, after which the train descended on a parachute. More comprehensive discussions on the replicator data have been presented by Heymsfield and Miloshevich (1993). High-resolution radiosonde data and position coordinates were obtained from the NCAR CLASS. During FIRE-II IFO, downward solar and IR radiative fluxes at the surface were continuously measured from broadband solar and IR flux radiometers operated by the National Oceanic and Atmospheric Administration. Further details on the calibration and deployment of the radiometers have been given in the Operational Plan of FIRE-II IFO (Fire Project Team 1991).

3. Retrieval analysis and verification methodology

a. Retrieval of cirrus cloud parameters

We have developed a retrieval scheme that uses radiance data of AVHRR 3.7-μm and 10.9-μm channels to determine cirrus temperature and thermal infrared (referred to as IR) emissivities based on the principle of radiative transfer and parameterizations. The retrieval scheme is based on the numerical solution of the following set of nonlinear algebraic equations (Ou et al. 1993):

$$R_i = (1 - \epsilon_i)R_{ai} + \epsilon_i B_i(T_c), \quad (1)$$

$$\epsilon_i = 1 - \exp(-k_i\tau), \quad i = 3, 4, \quad (2)$$

$$B_3(T_c) = \sum_{n=0}^{3} a_n[B_4(T_c)]^n, \quad (3)$$

where R_3 and R_4 are the upwelling radiances at the top of the atmosphere for the 3.7-μm and 10.9-μm channels for cirrus cloudy atmospheres, respectively; R_{a3} and R_{a4} are the corresponding radiances reaching the cloud base for the two channels; ϵ_3 and ϵ_4 are the cloud IR emissivities; T_c is the mean cirrus temperature; $B_3(T_c)$ and $B_4(T_c)$ are the Planck intensities at T_c; k_3 and k_4 represent the effective extinction coefficients for the two channels; and τ is the visible optical depth.

In the development, ϵ_3 and ϵ_4 are correlated by introducing the ratio k_4/k_3, which is a function of ice crystal size distribution. Based on the light scattering principle for hexagonal ice crystals (Liou et al. 1991), we have used a mean effective ice crystal size (D_e), defined as the mean ice crystal width weighted by the cross-sectional area, to represent ice crystal size distribution. Using a number of typical observed size distribution functions, a parameterization of k_4/k_3 in terms of mean effective size has been developed in conjunction with the cloud retrieval program.

Sensitivity studies on the effects of the variation in several cirrus parameters on upwelling radiances have been carried out. We find that the brightness temperature difference (BTD) between the 3.7-μm and 10.9-μm channels becomes larger for clouds with higher altitudes as well as for clouds containing small ice crystals, that the criterion BTD > 2 K is a good indicator of the presence of cirrus clouds, and that radiances from cirrus cloudy atmospheres depend significantly on k_4/k_3, the variation of which must be accounted for in the cirrus cloud retrieval program. Details of the sensitivity studies have been described in Ou et al. (1993). Finally, we have also constructed a relationship between cirrus temperature and mean effective ice crystal size, on the basis of cloud microphysics observations (see appendix).

b. Removal of the 3.7-μm solar component

During daytime, the 3.7-μm radiance contains both thermal emission and solar reflection. To apply the preceding retrieval program, we have developed an efficient but accurate scheme to remove the solar reflection part in the 3.7-μm radiance. This scheme is based on the correlations between 0.63-μm and 3.7-μm solar reflectances, which are obtained from the radiative transfer programs developed by Takano and Liou (1989b). These programs take into account the scattering and

absorption properties of nonspherical ice crystals for a range of mean effective ice crystal sizes and prescribed sun–satellite geometric parameters. The effects of the possible sources of errors on the retrieval results have been carefully analyzed in synthetic studies. Overall, the maximum percentage error in the 3.7-μm solar component that can occur in the removal scheme is less than 10% (Rao et al. 1995). We did not study the effects of ice crystal shapes on the removal accuracy, because it appears to us that the relationship between ice crystal shapes and the radiative properties of clouds will require considerable research before their impact on satellite remote sensing can be understood.

c. *Computation of cirrus visible optical depths and mean effective sizes from the replicator data*

To compute the cirrus visible optical depth from the replicator data, we must evaluate the cross sectional area A of an ice crystal. The photomicrograph obtained by the replicator contains signatures of various shapes of ice crystals. We divide these shapes of ice crystals into two groups and evaluate the ice crystal cross sections accordingly. For quasi-spherical and irregularly shaped ice crystals the cross-sectional area is expressed as the fraction (f) of the area occupied by the ice crystal within the circle circumscribing the crystal signature on a photomicrograph as follows:

$$A = \frac{\pi}{4} fL^2, \tag{4}$$

where L is the maximum dimension and $f = 0.9$ and 0.85 for quasi-spherical and irregularly shaped crystals, respectively, which are determined from photomicrograph data by eyeball examination.

For columns, bullets, rosettes, and plates, using a constant value of f in Eq. (4) will produce significant errors in A because the fraction f varies with crystal shapes. For this reason we use the expression derived by Takano and Liou (1989a) for randomly oriented hexagonal columns and plates:

$$A = \frac{3\sqrt{3}}{16} D^2 + \frac{3}{4} DL, \tag{5}$$

where D is the ice crystal width. It should be noted that the condition of random orientation is needed to account for different positions of columns and plates. Although in the real atmosphere ice crystals may show preferred orientations, the assumption of random orientation is applicable to the present analysis, since photomicrographs show that sampled ice crystals contain mainly aggregates, irregular and quasi-spherical particles, and that no exceptionally elongated or flat crystals were observed. For bullets and rosettes we derive a similar expression in the form

$$A = k\left(\frac{3\sqrt{3}}{16} \tilde{D}^2 + \frac{3}{4} \tilde{D}L\right), \tag{6}$$

where k is an empirical constant ($\sim$1.1) and $\tilde{D}$ is the width of an equivalent-area hexagonal crystal. The relationship between D and L developed by Auer and Veal (1970) has been used to compute A.

Once the cross-sectional area for each crystal in the photomicrograph is determined, the extinction coefficient for the visible wavelength can be obtained based on the principle of geometric optics as follows:

$$\beta_e = 2 \sum_{i=1}^{N} A_i n(L_i) \Delta L_i, \tag{7}$$

where A_i is the ice crystal cross-sectional area of the ith maximum-dimension interval, $n(L_i)$ is the number concentration of crystals that have maximum dimensions within the interval $L_i \pm \Delta L_i/2$, N is the total number of maximum-dimension intervals, and ΔL_i is the width of the ith interval. The visible optical depth τ is then computed from

$$\tau = \sum_{j=1}^{M} \beta_{ej} \Delta z_j, \tag{8}$$

where β_{ej} and Δz_j are the extinction coefficient and thickness, respectively, for the jth height interval.

To obtain the mean effective ice crystal size D_e from the replicator data, we adopt an indirect approach. The D_e for hexagonal crystals was defined in the form (Liou et al. 1991; Ou et al. 1993)

$$D_e = \int_{L_{\min}}^{L_{\max}} D^2 L n(L) dL \Big/ \int_{L_{\min}}^{L_{\max}} DL n(L) dL, \tag{9}$$

which is the mean width weighted by the cross section of ice crystals. This definition cannot be directly applied to quasi-spherical and irregularly shaped ice crystals. For this reason we relate D_e with the effective radius r_e of an equivalent-area sphere such that

$$r_e = \frac{\sum_{i=1}^{N} r_i^3 n(L_i) \Delta L_i}{\sum_{i=1}^{N} r_i^2 n(L_i) \Delta L_i}, \tag{10}$$

where

$$r_i = (A_i/\pi)^{1/2}. \tag{11}$$

We then correlate D_e and r_e using 11 measured size distribution functions for cirrus clouds that were obtained from the data presented by Heymsfield and Platt (1984) and Takano and Liou (1989a) and from the FIRE-I IFO aircraft 2D probe measurements (Fu and Liou 1993). Figure 1 shows the dependence of the computed D_e on r_e. The solid circle represents the com-

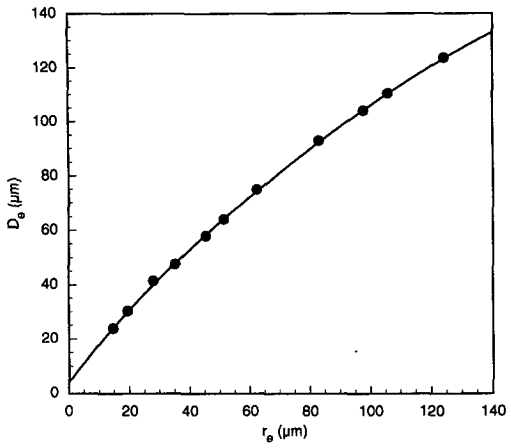

FIG. 1. Correlation between D_e and r_e using 11 measured ice crystal size distributions.

puted values based on the measured size distributions. We have developed a fourth-degree polynomial least square fitting for D_e in terms of r_e as follows:

$$D_e = \sum_{n=0}^{4} d_n r_e^n, \tag{12}$$

where $d_0 = 4.29263$, $d_1 = 1.48275$, $d_2 = -8.27388 \times 10^{-3}$, $d_3 = 5.04478 \times 10^{-5}$, and $d_4 = -1.43 \times 10^{-7}$. Based on Eqs. (10), (11), and (12), we can obtain the D_e values that are consistent with the definition of Eq. (9) for quasi-spherical and irregularly shaped ice crystals.

d. *Computation of downward surface radiative fluxes*

One of the potential applications of the retrieved cloud parameters is for the computation of the surface radiative budgets. In order to understand the role of land surface processes in global climate and climatic perturbations, the transport of radiative, latent heat, sensible heat, and chemical fluxes from the surface to the atmosphere must be determined over different types of surfaces as functions of various temporal and spatial scales. Remote sensing from satellites is the only means to provide routine observations of these fluxes on a global scale. Since clouds are the prime regulators of the radiative fluxes, uncertainties in the retrieved cloud parameters, which are inputs to radiative transfer models, can introduce significant errors in the computed radiative fluxes (Chou 1989). We use a detailed radiative transfer program involving a consistent representation of cloud fields and compute downward surface radiative fluxes under cirrus cloud conditions for different sets of microphysical properties. Comparisons are then made between the computed surface radiative fluxes and the ground-based radiometer measurements obtained during FIRE-II IFO.

The radiation parameterization program employed for the surface flux computations is based on the scheme developed by Fu and Liou (1992, 1993), specifically designed for applications to cirrus clouds. It integrates in a coherent manner the δ-four-stream approximation for radiative transfer, the correlated k-distribution method for nongray gaseous absorption, and the scattering and absorption properties of hexagonal ice crystals. We use the mean effective size, as defined previously, to account for the ice crystal size distribution with respect to radiation calculations.

The spectrally dependent extinction coefficient and single scattering albedo and the expansion coefficients in the phase function for the above-mentioned 11 observed ice crystal size distributions have been computed from a geometric ray-tracing technique for solid hexagonal columns and plates (size parameter > 30) (Takano and Liou 1989a) and a Mie-type solution for spheroids (size parameter < 30) (Takano et al. 1992). Using these results and basic physical reasoning, we have developed simple polynomial relationships between the single scattering properties and mean effective size (and ice water content) that can achieve relative accuracies within $\sim 1\%$. Note that the effects of ice crystals smaller than 20 μm on the single scattering properties have been accounted for in the parameterization. In the radiative transfer parameterization, a unified δ-four-stream approximation for both solar and IR flux calculations has been developed. With respect to the "exact" results computed from the adding method for radiative transfer, this scheme can yield relative accuracies within $\sim 5\%$ for all atmospheric conditions. The radiative transfer program described above has been demonstrated to be well suited for applications in cloudy conditions (Fu and Liou 1993).

The radiative transfer program requires the input of ice water content (IWC) and mean effective size (D_e). To obtain IWC, we employ the retrieved mean effective size and optical depth to obtain the mean ice water path (IWP) based on the following physical equation (Fu and Liou 1993):

$$\text{IWP} = \tau/(\alpha + \beta/D_e), \tag{13}$$

where α and β are certain constants. For the cloud thickness (Δz) we use the empirical equation obtained from lidar data developed by Platt et al. (1987) as follows:

$$\Delta z = \begin{cases} 0.0456T_c + 4.7, & -70°\text{C} < T_c < -35°\text{C} \\ -0.065T_c + 0.725, & -35°\text{C} < T_c < -10°\text{C}. \end{cases} \tag{14}$$

The vertically averaged IWC value is then given by

$$\text{IWC} = \text{IWP}/\Delta z. \tag{15}$$

Finally, the altitude of the cloud base and cloud top is determined from the estimated cloud thickness and the retrieved cloud temperature.

4. Results and discussions

As described previously, FIRE-II IFO over Coffeyville was carried out during November–December 1991 with a total number of 11 observed cirrus days (13, 17, 22, and 25–30 November and 5 and 6 December). Based on inspection of the available AVHRR data, replicator measurements, NCAR CLASS sounding data, and surface broadband radiative flux measurements, we find that the data collected during 26 November and 5 December are most appropriate for the present retrieval analyses and verifications for the following reasons. First, on both dates a layer of well-defined cirrus cloud was present over Coffeyville, so that the retrieval scheme, which was principally designed to retrieve the single-layer cloud properties, can be directly applied to the satellite data. Second, in both cases the temporal differences between the satellite overpass time and the replicator sampling time are small. The two datasets are therefore closely coincident and can be collocated in a Lagrangian sense. This part will be discussed further for each case.

a. The 5 December case

On this date, the sky was clear at sunrise and not very cold. A rapid influx of light cirrus (spissatus) was observed from the west during the morning. Coverage and density of cirrus increased through the day. Aircraft and ground-based sensors estimated cloud bases in the 10-km range, with tops extending to around 13 km. During the late afternoon, multilayered features covered the sky, with all stations in Kansas reporting high-level clouds. No low or middle level clouds passed over Coffeyville, but some low clouds were visible in the distant southern sky during the afternoon.

Figures 2a–c show the distribution of channel 4 brightness temperatures and the retrieved optical depths and mean effective ice crystal sizes over the 0.5° × 1.0° domain (36.75°–37.25°N, 94.8°–95.8°W) at 2100 UTC 5 December 1991, respectively. The symbol "+" denotes the location of Coffeyville. It is noted that almost the whole domain was covered with cirrus clouds. The distribution of the retrieved optical depths closely match that of the channel 4 brightness temperature. The cloud optical depth northeast of Coffeyville and near the southern boundary of the domain is larger than 3. However, the distribution of mean effective ice crystal sizes show no correlation with that of the channel 4 brightness temperature. Generally, the mean effective size increases from the south toward the north. The reliability of these retrieval results can only be confirmed by comparing them with independently derived observational data.

Figures 3a–e show the ice crystal size distributions derived from the replicator data at five selected height levels between the cloud base and cloud top. Near the cloud top (~13 km), the cirrus cloud is composed of small quasi-spherical particles ($L < 100$ μm). The smallest ice crystals that the replicator can measure are on the order of 5 μm. In the middle part of the cloud (9.8–12.0 km) there are columns, bullets, plates, and irregular particles. The size distributions become wider and more large particles appear in the lower part of the cloud. Near the 9.77-km level the size distribution is bimodal, where the larger mode is presumably due to the presence of large particles falling out from higher levels. Finally, near the cloud base (~9.6 km) there are only partially sublimated irregularly shaped ice crystals.

Because clouds are horizontally inhomogeneous, collocation and coincidence of the satellite data and replicator measurements in a Lagrangian sense are required for validation of the retrieval results. Figure 4 shows the geographical coordinates of the replicator at various times after launching. The replicator was launched at 2045 UTC and reached the cloud base and top at 2113 and 2125 UTC, or 5 and 17 min after the satellite overpass, respectively. These temporal differences are relatively small compared to the lifetime of cirrus clouds, which is on the order of several hours. We assume that the microphysical structure of the cloud remained largely unchanged during the period between the satellite overpass and the replicator sampling. Although there is no in situ data to confirm this assumption, simulation of ice crystal growth based on the theory of heat and vapor diffusional transport (Rogers and Yau 1989) support the assumption. To collocate the two datasets, we must determine the precise position of the cloudy region under the satellite overpass that was sampled by the replicator. In Fig. 4 the open and closed circles denote the coordinates of the sounding system when it reached the cloud base and top, respectively. Using the cloud-level windspeed and wind direction data recorded by the NCAR CLASS sounding system, we determine that at the time of satellite overpass the cloud associated with the replicator measurements was located at a position denoted by "x." This point near Coffeyville was upwind of the sounder positions at the cloud base and top because the satellite overpass was before the replicator sampling. Since the coordinates of this point are subject to uncertainties in the wind data, and to account for the possibility that the shear across the depth of the cloud may affect the vertical coherence over the period of interest, an area of 0.05° × 0.2° around this point is subsequently selected for the verification study.

Figures 5a and 5b show the averaged retrieval results within the 0.05° × 0.2° domain along with sounding measurements. Figure 5a displays the temperature and relative humidity profiles obtained from the NCAR CLASS sounding system between 2045 and 2129 UTC. The cloud base and top heights derived from the replicator sounding are 9.5 and 13 km. The relative humidity sharply increases with height near the cloud base and decreases upward above 10 km. The mean

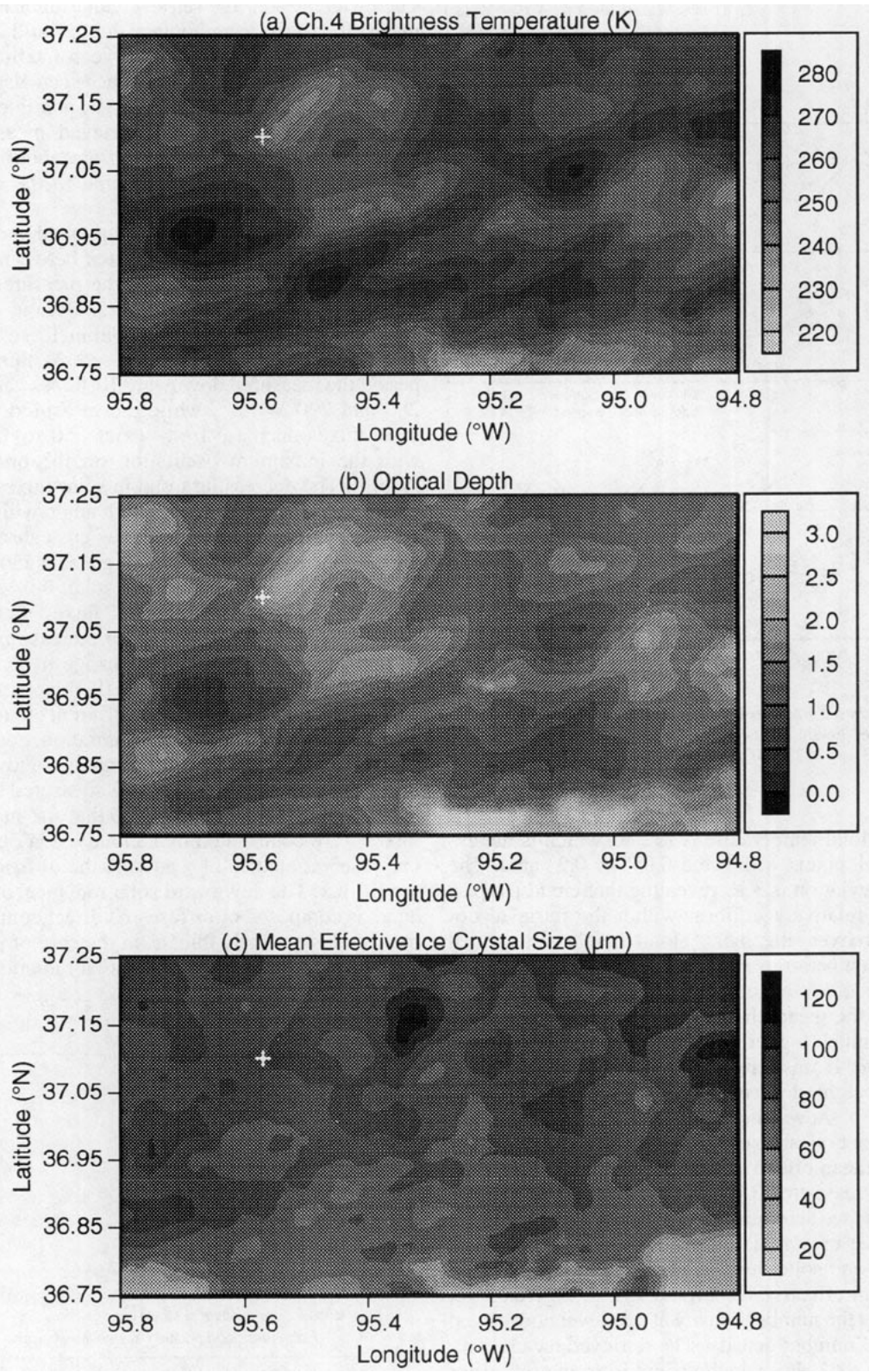

FIG. 2. Display of (a) AVHRR channel 4 brightness temperature, (b) the retrieved optical depth, and (c) the retrieved mean effective ice crystal size over a 0.5° × 1.0° area around Coffeyville, Kansas (denoted by the symbol "+"), at 2108 UTC 5 December 1991.

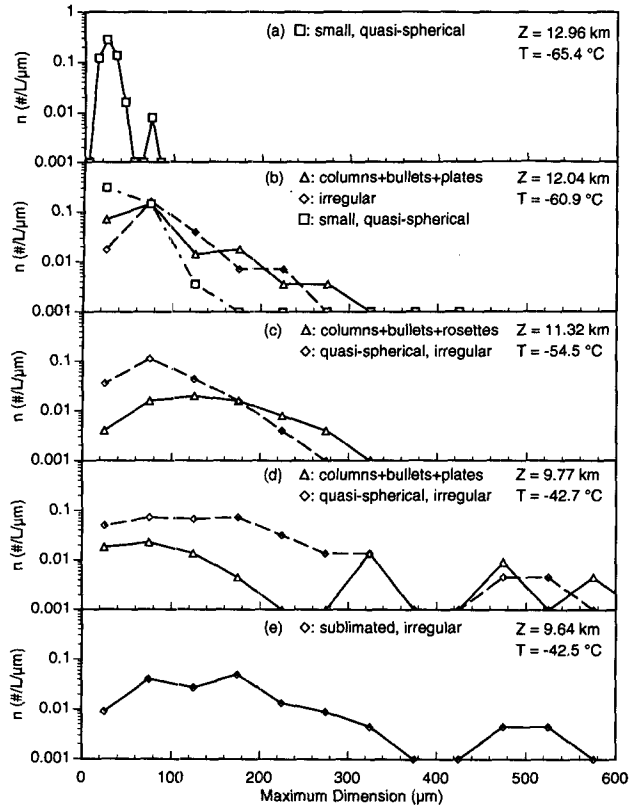

FIG. 3. Ice crystal size distributions derived from the replicator data at five selected height levels within the cloud, which was sampled between 2113 and 2125 UTC 5 December 1991.

retrieved cloud temperature is 212 K, which is the average of 81 pixels within the 0.05° × 0.2° area. The standard deviation is 3 K, revealing that cloud temperatures are relatively uniform within the retrieval domain. Moreover, the mean cloud height determined from the temperature sounding is 11.5 km, which is within the observed cloud boundaries. It should be noted that the mean channel 4 brightness temperature is 255 K, much higher than the mean retrieved cloud temperature. If this temperature were used to retrieve the cloud height, the error will be on the order of 6 km.

Figure 5b shows the vertical distribution of mean effective ice crystal sizes computed from the replicator data. The mean effective size is 15 μm near the cloud top and increases to 135 μm near the cloud base. From these values we determine the vertically averaged mean effective ice crystal size to be 97.3 μm, as shown in Fig. 5b by the solid vertical bar. This size is the sum of the mean effective ice crystal size at a given level weighed by the number density at that level normalized by the total number density. The retrieved mean effective size is 88.7 μm, which differs from the replicator value by less than 10 μm. On the bottom scale of Fig. 5b are shown the replicator-derived and the retrieved optical depths, which are 1.38 and 1.49, respectively. The differences in the retrieved and replicator-derived mean effective size and optical depth could well be due to the small time difference between satellite pass and replicator sounding. The differences can also be due to horizontal inhomogeneity. This is possible since the standard deviations of the retrieved mean effective sizes and optical depths, which are about 6 μm and 0.13, respectively, are comparable to the differences shown in Fig. 5b.

Figures 6a and 6b show the computed and measured downward surface radiative fluxes between 2000 and 2200 UTC. The accuracies of the measured radiative fluxes are within 5–10 W m^{-2} (J. DeLuisi 1993, personal communication). It is within these accuracies that computed results are assessed. Within this time period the measured downward IR fluxes vary between 280 and 290 W m^{-2}, while the measured downward solar fluxes decrease from about 350 to 100 W m^{-2} with the maximum oscillation on the order of 100 W m^{-2}. The decreasing trend in solar fluxes is mainly due to the increase in solar zenith angle with time. The greater variations of solar fluxes are caused by their higher sensitivity to the inhomogeneous cloud properties. Moreover, the pattern of solar flux oscillations does not match with that of IR fluxes. For example, near 2036 UTC there is a sharp increase in the solar fluxes with no corresponding change in IR fluxes observed. Note that the solar and IR fluxes measured at one point could be affected by different cloudy regions.

Based on the preceding consideration, great care has been taken to estimate the position of cloudy areas that affect the surface radiative fluxes measured by ground-based radiometers. We estimate that the measured IR fluxes were contributed by a cloudy area directly over the observational site because of the diffuse nature of the IR flux. The downward solar radiance, on the other hand, is composed of diffuse and direct components. If the cloud is optically thin, as in the case of most cirrus clouds, the directly transmitted solar radiation will con-

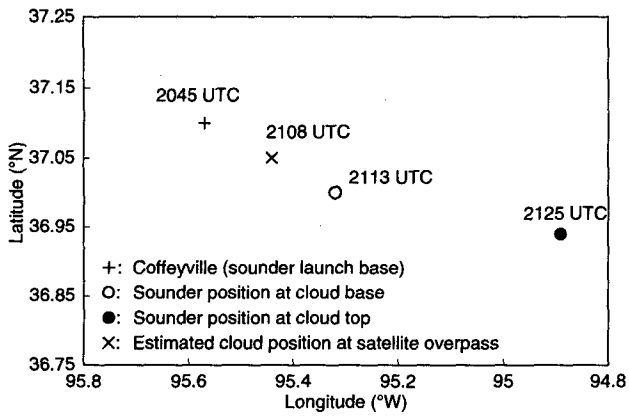

FIG. 4. Geographical coordinates of the replicator at various times after launching on 5 December 1991.

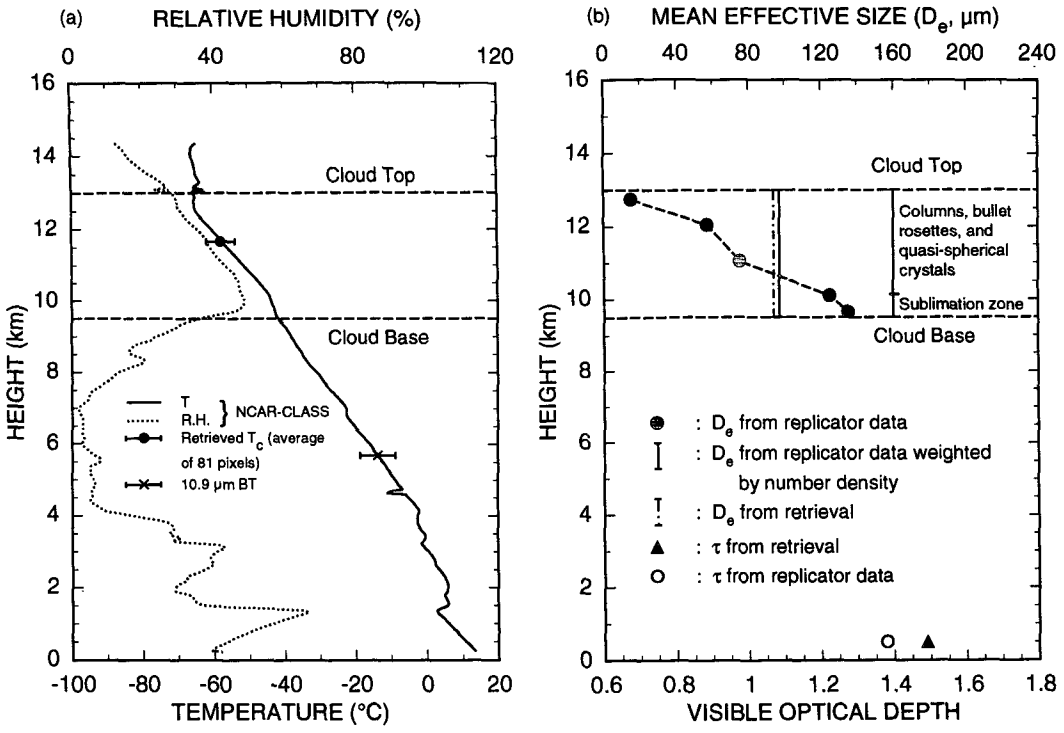

FIG. 5. (a) Temperature and humidity profiles obtained from the NCAR CLASS sounding system on 5 December 1991. Overlapped with the temperature profile are the mean retrieved cloud temperature and mean channel 4 brightness temperature over a 0.05° × 0.2° domain around Coffeyville. (b) Display of the replicator-derived mean effective sizes at the selected height levels, their vertical average, and the retrieved value. Also shown on the bottom scale are the optical depths derived from the replicator data and from the retrieval.

tribute significantly to the total flux. Therefore, the measured solar fluxes were contributed by a cloudy area centered around the direction of the incident solar radiation. For radiative fluxes measured before and after the satellite overpass, the associated cloudy areas would be located at different positions in the downwind and upwind directions at the time of the satellite overpass, respectively. Thus, we select several time periods within 30 minutes before and after the satellite overpass. Using the cloud-level wind speed and direction data recorded by the NCAR CLASS sounding system, we determine the location of the cloudy areas that are associated with the radiative fluxes measured at each time. A certain size of area around each estimated location is selected, and its mean cloud properties are determined from the removal–retrieval program for inputs into the radiative transfer model. The size of the selected area differs for IR and solar radiation. Since the distribution of downward IR radiance is diffuse, the contribution of radiance from the limb direction to the downward flux is significant. The direct solar component, on the other hand, should be primarily affected by the cloud property of the area centered at incident solar direction, as pointed out previously. In view of the above, we select a larger area for computing IR fluxes than for solar fluxes. For IR fluxes a 0.3° × 0.3° area is adequate because it contains clouds in the limb direction. For solar fluxes we find that a 0.1° × 0.1° area will suitably characterize the cloud property in the direction of incident solar radiation.

In Fig. 6a, the computed downward IR fluxes based on the mean satellite-retrieved cloud parameters over a 0.3° × 0.3° area around each estimated location agree reasonably well with ground-based measurements. Differences between the satellite-retrieved values and radiometer measurements are less than 5 W m^{-2} within 20 minutes before and after the satellite overpass. The computed radiative fluxes based on the mean effective ice crystal size, optical depth, and cloud top and base heights derived from the replicator data also closely match the measured values. However, if we use the cloud parameters based on climatological statistics (IWC = 0.005 g m^{-3}, D_e = 45 μm), errors in the computed IR fluxes are more than 10 W m^{-2}. Certain cloud retrieval scheme (e.g. ISCCP nighttime algorithm) treats cirrus clouds as thermally black. When a black cloud or clear-sky value is employed, much larger errors are produced. In Fig. 6b, the time series of both the retrieved and measured solar fluxes exhibit oscillation patterns. The computed solar fluxes based on the mean satellite-retrieved cloud parameters over a 0.1° × 0.1° area are lower than the measured values by less

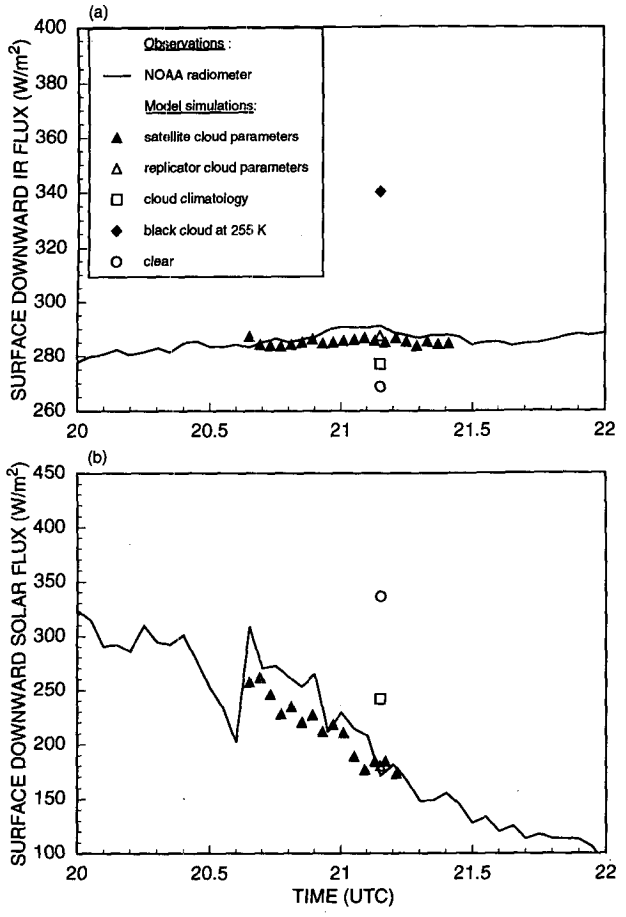

FIG. 6. Display of the measured and computed surface downward (a) IR and (b) solar radiative fluxes between 2000 and 2200 UTC 5 December 1991 at Coffeyville.

than 10%. These differences could be due to the inhomogeneity of the cloudy region as well as changes in cloud microphysical and optical properties during the time period between the ground-based measurements and satellite overpass. As in the case of IR fluxes, using the satellite-retrieved or replicator-derived cloud parameters leads to a better comparison with radiometer measurements than using climatological cloud data. The above comparisons of computed fluxes using different sets of cloud microphysical properties point to the need for accurate cloud information in determining surface radiation budget parameters.

b. The 26 November case

On this date clear and cold conditions existed over southeast Kansas at sunrise. Around noon cirrus spissatus began to spread over the area. By 1400 LST (2000 UTC), a broken cirrus layer was evident from 8.5 to 9.5 km, with increasing thickness. Lidars also reported a midlevel cloud layer (~6.5 km) at that time. Surface reports to the north and west indicated that clouds were located at multiple levels. By late afternoon, multilayered cloud conditions, including a low-level cloud deck, prevailed with continued strong southerly winds.

The *NOAA-11* passed Coffeyville at 0936 and 2111 UTC with viewing angles smaller than 30°. During the local nighttime overpass, the sky was clear. We have selected the *NOAA-11* data obtained during the 2111 UTC overpass for analysis. Figures 7a–c show the distribution of channel 4 brightness temperatures and the retrieved optical depths and mean effective sizes over a 0.5° × 1.0° domain (37.0°–37.5°N, 95.0°–96.0°W) around the region of FIRE-II IFO. The location of Coffeyville is again denoted by the symbol "+." From Fig. 7a, we observe that the whole domain is covered with clouds, except over the Coffeyville region and over the southeast corner. The distribution of the retrieved optical depths is similar to that of the channel 4 brightness temperature. The maximum optical depth is larger than 6 northwest of Coffeyville. The distribution of the mean effective sizes shows that smaller particles (~60 μm) are present around Coffeyville. The optical depths there are less than 1, indicating the presence of thin cirrus. Northeast of Coffeyville the retrieved optical depths are greater than 2, while the mean effective sizes are larger than 100 μm. This is the region that was sampled by the replicator.

Figures 8a–c show the size distributions derived from the replicator data at three selected height levels between cloud base and cloud top. Near the cloud top (~8.6 km, Fig. 8a) ice crystals are mostly irregularly shaped due to partial sublimation, and the number concentration is low. The maximum ice crystal dimensions are between 170 and 320 μm. It appears that this region is composed of residual particles from a layer of previously formed cirrus cloud at a higher altitude. Near the cloud center (~8 km) two types of ice crystals are present. The maximum dimension of irregularly shaped particles is between 20 and 440 μm. Their maximum number concentration is less than 0.1 L^{-1} μm^{-1}. On the other hand, the number concentration of smaller, quasi-spherical particles with maximum dimension between 20 and 100 μm is much higher. It is evident that this layer is composed of both newly formed small crystals and partially sublimated large crystals. Near the cloud base, highly sublimated irregularly shaped particles are present. The maximum ice crystal dimension is larger than 600 μm. The temperature dependence of ice crystal size distributions is not evident in this case because different stages of the ice-forming process occurred in the cloud. In middle levels the ice crystal characteristics are similar to those presented in the center diagram and thus are not shown here.

Figure 9 shows the geographical coordinates of the replicator at various time periods. The replicator was launched at 2025 UTC and reached the cloud base and top at 2046 and 2055 UTC, or 25 and 16 minutes before the satellite overpass (at 2111 UTC), respectively.

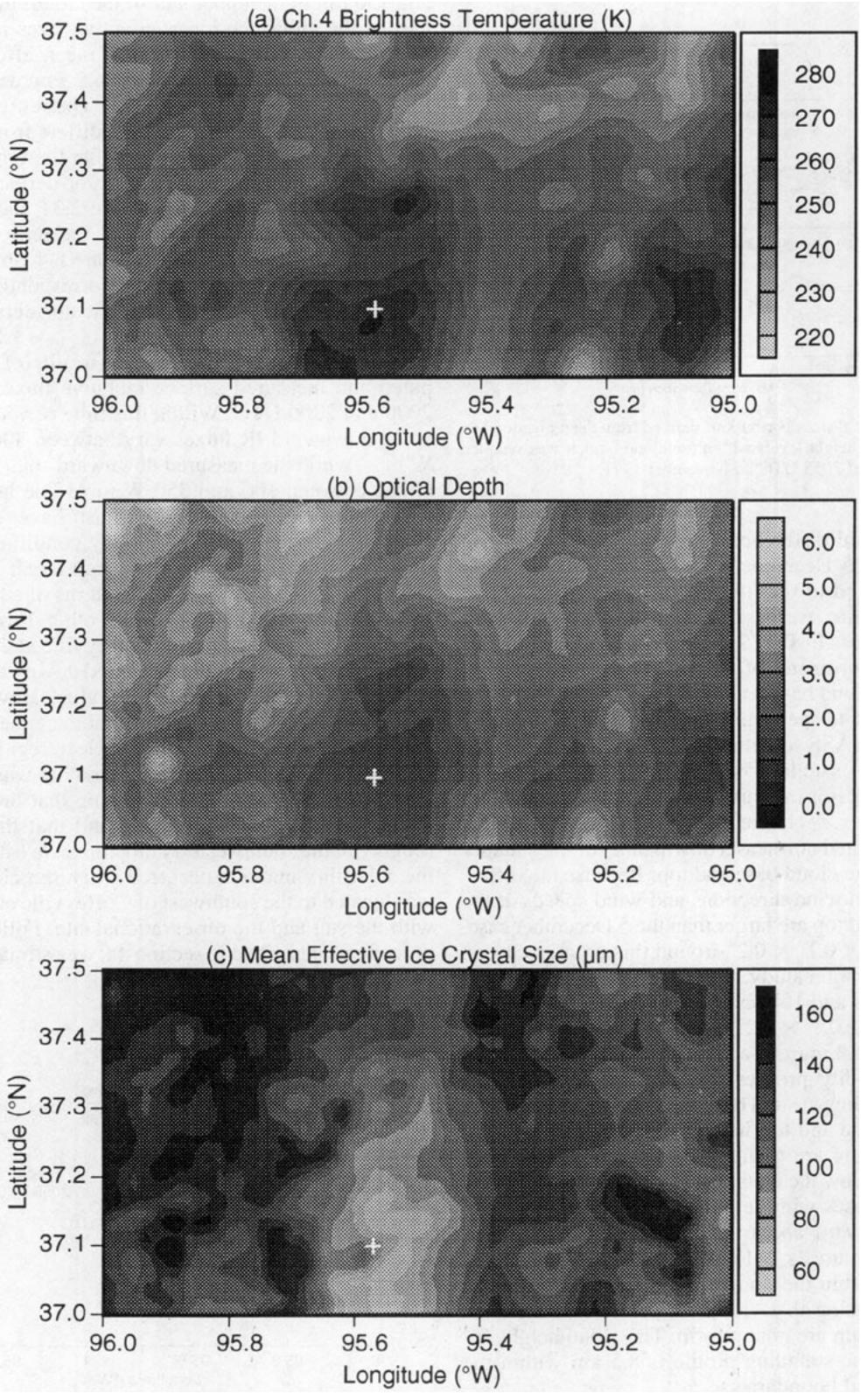

FIG. 7. As in Fig. 2 except over a different 0.5° × 1.0° area around Coffeyville, Kansas, at 2111 UTC 26 November 1991.

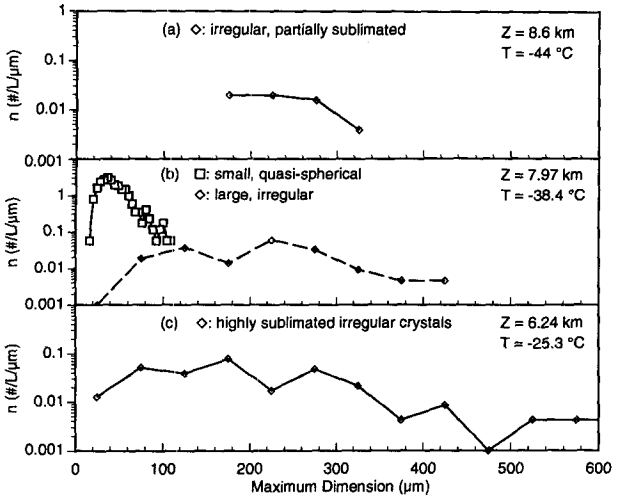

FIG. 8. Ice crystal size distributions derived from the replicator data at three selected height levels within the cloud, which was sampled between 2046 and 2055 UTC 26 November 1991.

These temporal differences are somewhat larger than those for the 5 December case but are still relatively small compared to the lifetime of cirrus clouds. Note that the satellite overpass is after the replicator sampling of clouds. In Fig. 9 the open and closed circles denote the coordinates of the sounding system when it reached the cloud base and top, respectively. Using the cloud-level wind speed and direction data recorded by the NCAR CLASS sounding system, we determine that at the time of satellite overpass the cloud associated with the replicator measurements moved to a position denoted by "x." Unlike the 5 December case, this point was located northeast (downwind) of the sounder positions at the cloud base and top. Because the differences between wind directions and wind speeds at the cloud base and top are larger than the 5 December case, a larger area of 0.1° × 0.2° around this point is chosen for the verification study.

Figures 10a and 10b show the averaged retrieval results within the 0.1° × 0.2° domain along with sounding measurements. Figure 10a displays the temperature and relative humidity profiles obtained from the NCAR CLASS sounding system between 2025 and 2105 UTC. The cloud base and top heights derived from the replicator sounding are 6 and 9 km. A few moist layers are present below the cloud base. The relative humidity sharply increases with height near the cloud base and decreases upward above 7 km. The mean retrieved cloud temperature is 231 K, which is the average of 148 pixels within the domain. The standard deviation is 7 K, indicating that cloud temperatures within the retrieval domain are nonuniform. The cloud height deduced from the sounding profile is 8.5 km within the observed cloud boundaries.

Figure 10b shows the vertical distribution of the mean effective ice crystal sizes computed from the replicator data. The mean effective size ranges between 80 and 130 μm in the upper half of the cloud. In the lower part of the cloud the mean effective sizes increase to 142 μm. The vertically averaged mean effective size based on the replicator data is 124.2 μm, as shown in Fig. 10b by the solid vertical bar. The retrieved mean effective size is 128.7 μm, which differs from the replicator value by less than 10 μm. On the bottom scale of Fig. 10b are shown the replicator-derived and the retrieved optical depths, which are 2.31 and 2.41, respectively. Standard deviations of the retrieved mean effective sizes and optical depths are 8.4 μm and 0.37 and are again comparable to the corresponding differences between retrieved and replicator-derived parametric values.

Figures 11a and 11b illustrate results of the computed and measured surface radiative fluxes between 2000 and 2200 UTC. Within this time period the measured downward IR fluxes vary between 300 and 360 W m^{-2}, while the measured downward solar fluxes oscillate between 100 and 350 W m^{-2}. The latter oscillation suggests that the sky must have drastically changed between clear and cloudy conditions. Variations for both IR and solar fluxes are larger than the 5 December case. Moreover, the patterns of solar and IR flux oscillations do not match each other. From Fig. 7a, there was a clear region over Coffeyville at the satellite overpass during which the measured downward IR flux reaches the expected minimum value. However, the time series of solar fluxes show that the expected maximum value associated with the clear region did not occur at the time of satellite overpass but was recorded about 20 minutes prior. Considering that the sun was to the southwest of Coffeyville and that the wind is roughly in the southwesterly direction, we estimate that the solar flux maxima occurred when the clear region was located to the southwest of Coffeyville and aligned with the sun and the observational site. Following the procedures described in section 4a, we estimate the part

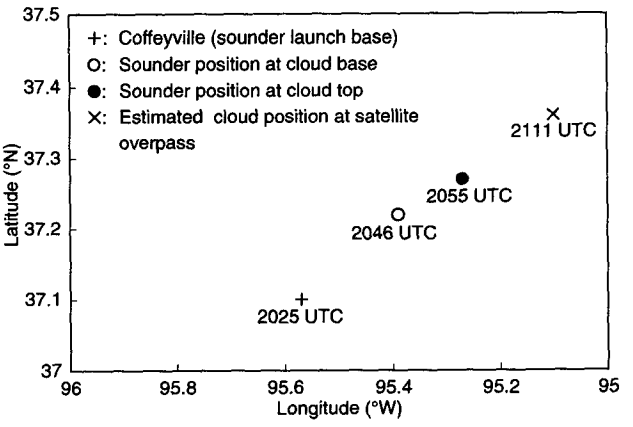

FIG. 9. Geographical coordinates of the replicator at various times after launching on 26 November 1991.

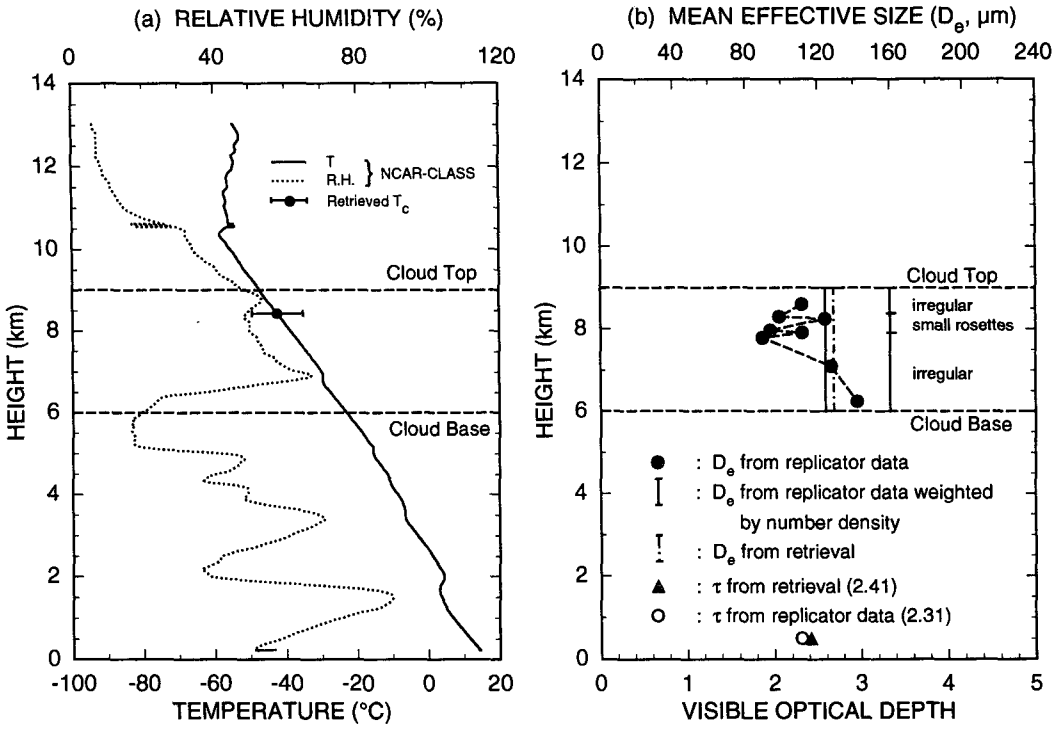

FIG. 10. As in Fig. 5 except for 26 November 1991.

of cloudy areas that would affect the surface radiative fluxes measured by ground-based radiometers and compute the radiative fluxes from the radiative transfer program.

In Fig. 11a the computed IR fluxes based on the mean satellite-retrieved cloud parameters over a 0.3° × 0.3° area around each estimated location differ from ground-based measurements by less than 5 W m^{-2} within 20 minutes before and after the satellite overpass. The computed IR fluxes based on the microphysical and geometrical parameters derived from the replicator data differ from the measured values by about 10 W m^{-2}. Use of the cloud parameters based on climatological statistics yields an IR flux that is also close to the observation. This is a coincidence because both the climatological IWC and D_e are smaller than the retrieved values so that the computed optical depth [Eq. (13)] is about the same as the retrieved optical depths. Again, if a black cloud or clear-sky values are used, significant errors occur in the computed IR fluxes. In Fig. 11b the computed time series of solar fluxes based on the mean retrieved cloud parameters over a 0.1° × 0.1° area exhibit a similar oscillation pattern to the observational time series. Good agreement between the computed and measured values is evident within ±5 minutes of satellite overpass and between 2040 and 2050 UTC. In addition, both the computed and measured time series of solar fluxes show maximum values between 2054 and 2106. However, based on relatively small values of optical depth (~0.6, compared to 2.31 shown in Fig. 10b), the computed fluxes are 20–100 W m^{-2} less than the measured value within this time period. These differences could be produced by the formation of cirrus cloud during the time period between the ground-based measurements and satellite overpass.

5. Conclusions

Recently, a removal–retrieval technique has been developed based on the theory of radiative transfer and parameterizations for the simultaneous removal of the solar component of the 3.7-μm radiance and the retrieval of cirrus cloud microphysical and optical parameters, using AVHRR visible and IR channel data (Ou et al. 1993; Rao et al. 1995). Some verifications of the retrieved cloud temperatures/heights from this scheme have been carried out using ground-based lidar measurements obtained during FIRE-I IFO. The retrieved optical depths have also been compared with the values determined from a different approach presented by Minnis et al. (1990a).

In this paper verifications of the retrieved cirrus optical depth and ice crystal sizes have been performed using balloonborne replicator and sounding data obtained during FIRE-II IFO. We have taken the advantage that the balloonborne replicator data can provide a nearly continuous vertical record of ice crystal size distributions in a Lagrangian sense. An analytical

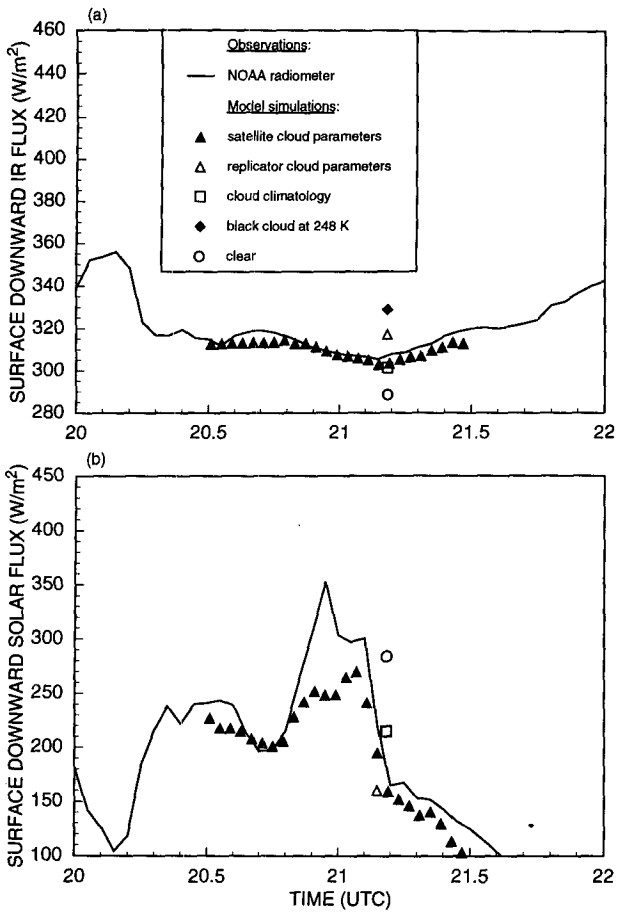

FIG. 11. As in Fig. 6 except for 26 November 1991.

method has been developed to derive the optical depth and the mean effective ice crystal size from the replicator data, taking into account the effects of different shapes, including quasi-spherical, irregular, and hexagonal ice crystals. Moreover, we apply the retrieved cloud properties to the computation of surface radiative fluxes using a radiative transfer program that involves a consistent representation of cloud fields and compare the computed values with data measured from ground-based radiometers.

We have focused on the cases of 26 November and 5 December. On both dates a well-defined cirrus layer was present over the Coffeyville area, and the temporal differences between the satellite overpass and the replicator sampling are small. The two datasets are closely coincident and can be collocated in a Lagrangian sense. In each case we first perform retrievals over a 0.5° × 1.0° region around the Coffeyville area and obtain the distribution of cloud optical depth and mean effective size. We then determine the approximate position of the cloudy region that was sampled by the replicator under the satellite overpass. A small area around this position is subsequently chosen, and the mean retrieved cloud parameters of this domain are compared with those derived from the replicator and sounding data. We show that the retrieved cirrus cloud temperature, mean effective size, and optical depth closely match with the values determined from sounding and replicator data. Differences in the retrieved and replicator-derived values of the cloud parameters could be a result of the small temporal differences between the satellite pass and replicator sounding.

To verify the computed radiative fluxes, we have carefully estimated the position of cloudy areas that affect the surface radiative fluxes measured by the ground-based measurements. We show that the computed downward surface solar and IR fluxes are within 10 and 5 W m^{-2}, respectively, of the ground-based measurements near the time of satellite overpass. These differences could be caused by the inhomogeneity of the cloudy region as well as changes in the cloud microphysical and optical properties during the time period between the ground-based measurements and satellite overpass, and the uncertainties in measured radiative fluxes (5–10 W m^{-2}). Although we have initial success in the validation of surface radiative fluxes determined from satellite retrieval/radiation models, several relevant issues need to be further explored in future works, including the collocation of NOAA satellite overpasses and ground-based radiometric measurements, the averaging of satellite-retrieved pixel fluxes over appropriate cloudy areas, the importance of aerosol contributions in surface flux calculations in cirrus cloudy atmospheres, and the limitation of satellite retrievals/radiation model calculations for surface fluxes in cirrus cloudy conditions.

Acknowledgments. This research work was supported by NASA Grants NAG5-1050 and NAG1-1719, and in part by Air Force Contracts F19628-92-K-0019 and F19628-95-K-002. Information to FIRE data summary was provided by Dr. K. Sassen.

APPENDIX

Effective Mean Ice Crystal Size and Cloud Temperature

A direct determination of D_e from the data that are available from the present satellite thermal infrared radiometers appears to be very difficult, if not impossible. However, we may relate D_e to the cloud temperature through appropriate observations. Based on a large number of cirrus microphysical data collected by optical probes during flights over midlatitudes, Heymsfield and Platt (1984) have suggested that ice crystal size distribution can be represented by a general power form as follows:

$$n(L) = \begin{cases} A_1 L^{b_1}(\mathrm{IWC}), & L \leqslant L_0 \\ A_2 L^{b_2}(\mathrm{IWC}), & L > L_0, \end{cases} \quad \text{(A1)}$$

where $L_0 = (A_2/A_1)^{1/(b_1-b_2)}$, IWC is the ice water content, and $A_{1,2}$ and $b_{1,2}$ are empirical coefficients deter-

mined from the measured data. Heymsfield and Platt (1984) have shown that for a given temperature values of $A_{1,2}$, $b_{1,2}$, and IWC are subject to uncertainties due to the observational data spread. However, the mean values of $A_{1,2}$, $b_{1,2}$, and IWC may be parameterized in terms of temperature in the range of $-20°$ to $-60°$C (Liou 1992). Based on this parameterization, the mean $n(L)$ is also a function of temperature. Moreover, aircraft and laboratory measurements indicate that the width D and the length L of a hexagonal ice crystal are related (e.g., see Auer and Veal 1970) in which a parameterization relation can be developed for the two. Thus, with the functional form of $n(L)$ determined, the temperature-dependent mean effective size $\bar{D}_e$ can be obtained, where the overbar denotes the mean value for a given temperature. Subsequently, we perform a least squares polynomial fitting to relate $\bar{D}_e$ to T_c in the form

$$\bar{D}_e = \sum_{n=0}^{3} c_n (T_c - 273)^n, \qquad \text{(A2)}$$

where $c_0 = 326.3$, $c_1 = 12.42$, $c_2 = 0.197$, and $c_3 = 0.0012$. Equation (A2) was used in our previous retrievals (Ou et al. 1993; Rao et al. 1994).

The retrieved $\bar{D}_e$ may be in error due to uncertainties in $A_{1,2}$, $b_{1,2}$, and IWC. To improve the accuracy of the retrieved mean effective size, we modify the value of $\bar{D}_e$ according to the following procedures. Let D_e be the modified value of $\bar{D}_e$, and let D_e and $\bar{D}_e$ differ by a factor of c as follows:

$$D_e = c\bar{D}_e. \qquad \text{(A3)}$$

The factor c is to be obtained from the relationship between D_e and IWC. We assume that D_e and IWC have the following relationship based on dimensional analysis:

$$D_e \propto (\text{IWC})^{1/3}. \qquad \text{(A4)}$$

Observational evidence (Heymsfield and Platt 1984) shows that

$$\bar{D}_e \propto (\overline{\text{IWC}})^{1/3}, \qquad \text{(A5)}$$

where $\overline{\text{IWC}}$ is the temperature-dependent mean value of IWC, derived from observations. According to Liou (1992), $\overline{\text{IWC}}$ can be parameterized in terms of T_c as follows:

$$\overline{\text{IWC}} = \exp\{-7.6 + 4\exp[-0.2443 \times 10^{-3}(253 - T_c)]^{2.445}\}, \quad \text{for } T_c < 253 \text{ K}. \qquad \text{(A6)}$$

The quantity IWC may be expressed by (Fu and Liou 1993)

$$\text{IWC} = \tau/[\Delta z(\alpha + \beta/D_e)], \qquad \text{(A7)}$$

where τ is the visible optical depth, Δz is the cloud thickness, and α and β are empirical constants. Substituting Eqs. (A4)–(A7) into Eq. (A3), and assuming that the proportional constants in Eqs. (A4) and (A5) are the same, we obtain

$$D_e = [\tau/\Delta z(\alpha + \beta/D_e)\overline{\text{IWC}}]^{1/3}\bar{D}_e. \qquad \text{(A8)}$$

Equation (A8) is an implicit algebraic equation for D_e. To solve Eq. (A8), we first determine $\overline{\text{IWC}}$ and $\bar{D}_e$ from Eqs. (A2) and (A6), respectively, using the retrieved cloud temperatures. Subsequently, we solve for D_e numerically based on the retrieved value of τ and the prescribed value of Δz.

Equation (A8) has been verified using the balloon-borne replicator data collected on 26 November and 5 December 1991 during FIRE-II IFO (see sections 2 and 4). We compute D_e from Eq. (A8) for each sampled level shown in Figs. 5b and 10b, where $\tau/\Delta z$ is replaced by the extinction coefficient β_e from Eq. (7) and $\overline{\text{IWC}}$ and $\bar{D}_e$ are determined based on the level temperature from Eqs. (A2) and (A6), respectively. Table A1 shows the vertically averaged D_e values, which are obtained in the same way as the vertically averaged D_e derived from the replicator data (Figs. 5b and 10b). Also shown in Table A1 are the replicator-derived D_e. It is noted that computed D_e differ from replicator-derived values by no more than 10 μm. This comparison demonstrates that for both cases shown here Eq. (A8) is a good parameterization.

TABLE A1. Vertically averaged values of D_e from Eq. (A8), compared with replicator-derived D_e.

Date	D_e [Eq. (A8)]	D_e (replicator)
26 Nov	90.0	97.3
5 Dec	134.0	124.2

REFERENCES

Auer, A. H., Jr., and D. L. Veal, 1970: The dimension of ice crystals in natural clouds. *J. Atmos. Sci.*, **27**, 919–926.

Baum, B. A., T. Uttal, M. Peollot, T. P. Ackerman, J. M. Alvarez, J. Intrieri, D. O'C. Starr, J. Titlow, V. Tevinkere, and E. Clothiaux, 1994: Satellite remote sensing of multiple cloud layers. *J. Atmos. Sci.*, **52**, 4210–4230.

Chou, M. D., 1989: On the estimation of surface radiation using satellite data. *Theor. Appl. Climatol.*, **40**, 25–36.

Fire Project Team, 1991: FIRE Cirrus Intensive Field Observations—II: Operations Plan. FIRE Project Office and the FIRE Cirrus Working Group, 116 pp.

Fu, Q., and K. N. Liou, 1992: On the correlated k-distribution method for radiative transfer in nonhomogeneous atmospheres. *J. Atmos. Sci.*, **49**, 2139–2156.

——, and ——, 1993: Parameterization of the radiative properties of cirrus clouds. *J. Atmos. Sci.*, **50**, 2008–2025.

Heymsfield, A. J., and C. M. R. Platt, 1984: A parameterization of the particle size spectrum of ice clouds in terms of the ambient temperature and the ice water content. *J. Atmos. Sci.*, **41**, 846–855.

——, and L. M. Miloshevich, 1993: Overview of microphysics and state parameter measurements from FIRE-II. *Proc. Conf. on FIRE Cirrus Results*, Breckenridge, CO, NASA 1–4.

Kidwell, K. B., 1991: *NOAA Polar Orbitter Data Users Guide.* 280 pp. [Available from NOAA National Climatic Data Center, Satellite Data Services Division, Princeton Executive Square, Room 100, Washington, D.C.]

Liou, K. N., 1986: Influence of cirrus clouds on weather and climate processes: A global perspective. *Mon. Wea. Rev.,* **114,** 1167–1199.

——, 1992: *Radiation and Cloud Processes in the Atmosphere: Theory, Observation, and Modeling.* Oxford University Press, 487 pp.

——, J. L. Lee, S. C. Ou, Q. Fu, and Y. Takano, 1991: Ice cloud microphysics, radiative transfer and large-scale cloud processes. *Meteor. Atmos. Phys.,* **46,** 41–50.

Magono, C., and S. Tazawa, 1966: Design of "Snow Crystal Sondes." *J. Atmos. Sci.,* **23,** 618–625.

Minnis, P., D. F. Young, K. Sassen, J. M. Alvarez, and C. J. Grund, 1990a: The 27–28 October 1986 FIRE IFO cirrus case study: Cirrus parameter relationships derived from satellite and lidar data. *Mon. Wea. Rev.,* **118,** 2402–2425.

——, P. W. Heck, and E. F. Harrison, 1990b: The 27–28 October 1986 FIRE IFO cirrus case study: Cloud parameter fields derived from satellite data. *Mon. Wea. Rev.,* **118,** 2426–2446.

——, ——, and D. F. Young, 1993: Inference of cirrus cloud properties from satellite-observed visible and infrared radiances. Part II: Verification of theoretical cirrus radiative properties. *J. Atmos. Sci.,* **50,** 1305–1322.

Ou, S. C., K. N. Liou, W. M. Gooch, and Y. Takano, 1993: Remote sensing of cirrus cloud parameters using advanced very-high-resolution radiometer 3.7- and 10.9-μm channels. *Appl. Opt.,* **32,** 2171–2180.

Platt, C. M. R., J. C. Scott, and A. C. Dilley, 1987: Remote sounding of high clouds. Part VI: Optical properties of midlatitude and tropical cirrus. *J. Atmos. Sci.,* **44,** 729–747.

Rao, N. X., S. C. Ou, and K. N. Liou, 1995: Removal of the solar component in AVHRR 3.7-μm radiances for the retrieval of cirrus cloud parameters. *J. Appl. Meteor.,* **34,** 482–499.

Rogers, R. R., and M. K. Yau, 1989: *A Short Course in Cloud Physics.* Pergamon Press, 293 pp.

Schaefer, V., 1941: A method for making snowflake replicas. *Science,* **93,** 239–240.

Takano, Y., and K. N. Liou, 1989a: Radiative transfer in cirrus clouds. Part I: Single-scattering and optical properties of oriented hexagonal ice crystals. *J. Atmos. Sci.,* **46,** 3–19.

——, and ——, 1989b: Radiative transfer in cirrus clouds. Part II: Theory and computation of multiple scattering in an anisotropic medium. *J. Atmos. Sci.,* **46,** 20–38.

——, ——, and P. Minnis, 1992: The effects of small ice crystals on cirrus infrared radiative properties. *J. Atmos. Sci.,* **49,** 1487–1493.

Weinreb, M. P., G. Hamilton, and S. Brown, 1990: Nonlinearity corrections in calibration of Advanced Very High Resolution Radiometer infrared channels. *J. Geophys. Res.,* **95,** 7381–7388.

Whitlock, C. H., and Collaborators, 1990: AVHRR and VISSR satellite instrument calibration results for both cirrus and marine stratocumulus IFO periods. NASA Conf. Publ. 3083, 141–146.